Active hyperpolarization of the nuclear spin lattice: Application to hexagonal boron nitride color centers

F. T. Tabesh [1,*] M. Fani [1] J. S. Pedernales,[2] M. B. Plenio,[2] and M. Abdi[1,†]
[1]*Department of Physics, Isfahan University of Technology, Isfahan 84156-83111, Iran*
[2]*Institut für Theoretische Physik, Albert-Einstein-Allee 11, Universität Ulm, 89069 Ulm, Germany*

(Received 11 October 2022; revised 18 May 2023; accepted 5 June 2023; published 16 June 2023)

The hyperpolarization of nuclear spin ensembles through their interaction with optically active color centers has emerged as a promising technique with applications ranging from sensing and imaging to quantum computation. Here, we investigate the efficiency of this approach for the hyperpolarization of the nuclear-spin bath in a monolayer of hexagonal boron nitride via the optically active boron vacancy centers (V_B). To that end we design a polarization sequence based on the suitable combination of optical polarization and microwave driving of the V_B, which we optimize numerically. To extend our study to realistic systems with a large number of interacting spins, we employ an approximate method based on the Holstein-Primakoff transformation, whose validity we benchmark against exact numerics for small system sizes. Our results suggest that a high-degree of polarization in the boron and nitrogen nuclear-spin lattices is achievable also at room temperature. Our work provides the first step toward the realization of a two-dimensional quantum simulator based on natural nuclear spins and it can prove useful for extending the coherence time of the V_B centers.

DOI: 10.1103/PhysRevB.107.214307

I. INTRODUCTION

Color centers, also known as point defects, are atomic or molecular sites within a crystal lattice that can absorb and emit light at specific wavelengths [1]. They have garnered considerable attention in recent years due to their potential use in a variety of quantum technologies, including quantum computing, quantum communication, and quantum sensing. This is because some color centers, such as the nitrogen-vacancy (NV) centers in diamond [2] and different defects in silicon carbide [3,4], exhibit long coherence times, strong optical interactions, and room-temperature operation, which make them promising candidates for developing new quantum devices. In particular, it has been identified that electron spins of defect centers in wide-band-gap semiconductors, most notably diamond, can be initialized optically and controlled by microwaves [2]. In addition, the controlled coupling of these electron spins to proximal nuclear spins (of, e.g., nitrogen atoms for the NV-center cases or ^{13}C) has been achieved using microwave pulses [5] and electrical [6] or optical detection [7].

On the other hand, extended systems such as nuclear spins on the surface of diamond [8] or thin ^{13}C layers in diamond [9] have been recently proposed as potential quantum simulators. However, a key challenge of these implementations is the initialization of such nuclear-spin ensembles, i.e., generation of a robust hyperpolarized state with nearly 100% spin polarization [8,9]. Various methods have been studied to achieve this high level of spin polarization by employing color centers in diamond [8,10–16] and in silicon carbide [17]. For example, the highly controllable color centers can be polarized efficiently at room temperature via optical and microwave drives, and their polarization can be transferred to other interacting spin systems.

In spite of the various valuable works on NV centers in diamond, spin defects in noncarbon lattices have mostly been overlooked, while there are tremendous unexplored areas outside the carbon realm. More recently, defect centers in 2D materials such as hexagonal boron nitride (hBN) have been identified experimentally [18–21] and characterized theoretically [22,23]. In this case, due to the simultaneous presence of different nuclear-spin species in the lattice structure, the initialization of the spin ensemble is more complex. Recently, the first experimental attempts to polarize the spin ensemble in hBN have been reported [24]. These are based on the operation of the color center close to its ground-state level anticrossing, which allows for polarization transfer to the nuclear-spin ensemble. In this paper, we explore an alternative approach that, inspired by the hyperpolarization of ^{13}C nuclear spins in diamond, is based on the microwave control of the color center and provides a potentially scalable scheme for the hyperpolarization of the nuclear spins in hBN.

Here, we study the hyperpolarization of nuclear spins (boron and nitrogen) in a monolayer of hBN via electromagnetic manipulation of the electron spin of V_B. As an immediate application, this can significantly decrease the pure dephasing contribution of the spin bath, and thus enhance the coherence time of the defect spin state. A longer coherence time shall prove useful in every follow-up quantum technological application, see, e.g., Ref. [25]. Unlike the hyperpolarization of the nuclear spins in diamond, here one should deal with the polarization of two sublattices with different nuclear species and different spin values. We analyze the hyperpolarization of the hBN lattice by optical pumping and microwave driving and find a rapid and efficient

*fatemeh.tabesh@gmail.com
†mehabdi@gmail.com

performance reaching levels of polarization well beyond the thermal polarization, even at low-temperatures and high magnetic fields. In particular, we examine the direct polarization swap between the V_B defect and the surrounding nuclei by applying a microwave field to drive the electron spin of the V_B defect. In this scheme, the population transfer takes place when the Rabi frequency of the microwave driving field is resonant with the energy splitting of the nuclear spins. Therefore, the flip-flop processes between the V_B defect and the nuclear spins can result in the polarization of the nuclear-spin lattice. Moreover, we optimize the performance of our protocol by adjusting the magnetic-field orientation as well as the frequency and amplitude of the microwave drive.

To corroborate our study with numerical analyses on such large spin systems, we employ an approximate numerical method that overcomes the typical limitations in computational resources for dealing with large-scale spin systems. The numerical method is based on using a bosonic approximation through the Holstein-Primakoff (HP) transformation [26]. We justify the validity of the approximation in the working regime of our interest by benchmarking its results with the exact numerics for small-sized lattices. The study is then extended to larger lattices with faster and yet considerably less computational resources. The HP transformation has been used for investigating hyperpolarization of oil molecules [13], sensing phases of water via NV centers [27], and simulating a diamond surface [8].

Before addressing the hBN problem, we explore the strengths and limitations of the employed numerical bosonic method and examine the range of its validity by applying it to the simpler, inhomogeneous, central-spin model. In this toy model, the spins in a one-dimensional Heisenberg chain inhomogeneously interact with a distinct spin, the "central spin." We argue that the bosonic approach is in good agreement with exact numerical simulation if the interaction between the central spin and the spin bath is long range. Also, we find that the interaction among bath spins plays an effective role to transfer polarization throughout the one-dimensional lattice. This, together with the description of the Heisenberg model and the Gaussian state method, is described in Sec. II. In it, we study the strong polarization of the spin ensemble by driving the central spin and compare the results of the exact solution with those of the bosonic approximation for a system of reduced size. In Sec. III, we introduce the Hamiltonian of hBN lattice with a negatively charged V_B defect and the nuclear bath model and study the hyperpolarization of this lattice applying the methods developed in Sec. II. Finally, we summarize and conclude in Sec. IV.

II. CENTRAL SPIN MODEL

To better understand the hyperpolarization process through active manipulation of a defect spin and to examine the area of validity of the employed approximate numerical method, here we investigate the familiar problem of central spin model.

A. Hamiltonian

We begin with the nearest-neighbor Heisenberg model for a chain of one-half spins [28–30] described by the

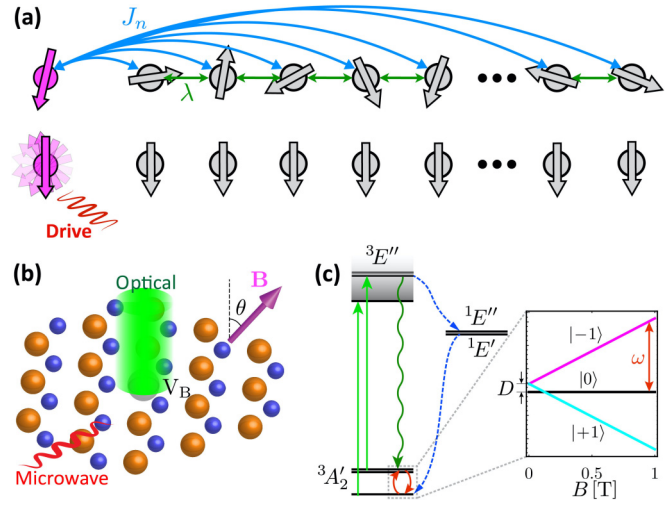

FIG. 1. (a) Sketch of the central spin model studied in this work (top panel) and the hyperpolarization of the bath spin chain as a result of the active manipulation of the control spin (bottom panel). (b) The geometry of the V_B defect in hBN: A negatively charged boron vacancy (gray) surrounded by nitrogen (blue) and boron (orange) atoms. The optical polarizing and microwave drives are also indicated. (c) V_B defect simplified energy-level diagram: The straight green lines show the exciting laser transitions, while the curly green and dashed blue lines denote the radiative and nonradiative decay to the ground state, respectively. The red circle arrows represents the microwave drive. The inset presents a closer look at the ground-state manifold and its manipulation via external magnetic field and microwave drive.

Hamiltonian ($\hbar = 1$)

$$\hat{H}_B = h\sum_{n=1}^{N}\hat{S}_n^z + \lambda\sum_{n=1}^{N-1}\left(\hat{S}_n^z\hat{S}_{n+1}^z + \hat{S}_n^+\hat{S}_{n+1}^- + \hat{S}_n^-\hat{S}_{n+1}^+\right), \quad (1)$$

where $\hat{S}_n^z = \frac{1}{2}\sigma_n^z$ denotes the spin operator in the z direction and $\hat{S}_n^+$ ($\hat{S}_n^-$) is the raising (lowering) operator for site n. Here, h is the Larmor frequency, which is proportional to the background magnetic field, and λ is the coupling strength. The first term of Hamiltonian (1) is the free energy of spins and the second term describes the nearest-neighbor one-dimensional interactions among the spins. At zero temperature and in the limit of $\lambda \ll h$, the ground state of the system is unique and given by $|\mathbf{0}\rangle = |0\rangle^{\otimes N}$, where $|0\rangle$ and $|1\rangle$ are the eigenstates of σ^z (Pauli matrix in the z direction), respectively corresponding to -1 and $+1$.

Now we consider a central spin-one-half particle as the control quantum entity, whose free dynamics is described by the Hamiltonian $\hat{H}_{cs} = \omega_0\hat{s}^z$ with Larmor frequency ω_0. In a possible realistic physical implementation, the control spin is an optically active spin to which a resonant driving field is applied for its manipulation, see Fig. 1(a). The central (control) spin interacts with the Heisenberg chain through the following Hamiltonian:

$$\hat{H}_{int} = \sum_{n=1}^{N} J_n\hat{s}^x\hat{S}_n^x, \quad (2)$$

where J_n are the long-range coupling strengths, while $\hat{s}^z$ and $\hat{s}^x$ are the spin operators of the control spin. The whole system dynamics is thus given by the Hamiltonian $\hat{H} = \hat{H}_{\rm cs} + \hat{H}_{\rm B} + \hat{H}_{\rm int}$.

For the sake of simplicity, we assume that $\lambda, J_n \ll h, \omega_0$. Hence, the conditions for the rotating-wave approximation (RWA) are safely satisfied and the total Hamiltonian reads

$$\hat{H} = \omega_0 \hat{s}^z + h\sum_{n=1}^{N} \hat{S}_n^z + \lambda \sum_{n=1}^{N-1} \left(\hat{S}_n^z \hat{S}_{n+1}^z + \hat{S}_n^+ \hat{S}_{n+1}^- + \hat{S}_n^- \hat{S}_{n+1}^+\right) + \sum_{n=1}^{N} J_n(\hat{s}^+ \hat{S}_n^- + \hat{s}^- \hat{S}_n^+), \quad (3)$$

where the second line of the above Hamiltonian represents the flip-flop interactions between the control spin and Heisenberg chain spins.

B. Hyperpolarization

The hyperpolarization of the spin chain can be achieved by cyclically polarizing the color central spin and transferring this polarization to the rest of the spins in the chain via the flip-flop interaction. In this scheme, a single cycle consists of the following steps: (i) The control spin is initialized in the $|0\rangle$ state. This can be done, e.g., by applying a laser pulse. (ii) The control spin is driven in resonance with the "bath" spins, such that the Hartmann-Hahn condition is satisfied and, thus, the polarization of the control spin is transferred to the bath spins [31]. The frequency tuning of the control spin for satisfying the resonance condition can be done in various ways. One possibility is to apply a resonant driving field with a proper Rabi frequency, see Sec. III. The two above polarizing steps are repeated as many as necessary times to achieve the desired level of polarization in the Heisenberg chain spins. To put it in the mathematical form, the total initial state is given by $\rho(0) = |0\rangle\langle 0|_{\rm cs} \bigotimes_{n=1}^{N} \rho_n^{\rm th}$ where $\rho_n^{\rm th}$ is the initial unpolarized thermal state of the nth spin in the chain. After the $(R+1)$st iteration of the polarization cycle, the state of the Heisenberg spins is found by

$$\hat{\rho}_{\rm B}((R+1)\tau) = {\rm Tr}_{\rm cs}\{\hat{U}(\tau)[|0\rangle\langle 0|_{\rm cs} \otimes \hat{\rho}_{\rm B}(R\tau)]\hat{U}^\dagger(\tau)\}, \quad (4)$$

where $\hat{U}(t) \equiv \exp\{-i\hat{H}t\}$ is the time evolution operator with $\hat{H}$ being the Hamiltonian in Eq. (3) and ${\rm Tr}_{\rm cs}\{\}$ indicates the partial trace over the control spin. Here, the period of all cycles is taken to be identical and equal to τ. We must emphasize that the polarization can be effectively transferred from the control spin to the Heisenberg spins when $\omega_0 = h$. Thus, ideally, after a sufficient number of cycles the final state of the bath spins approaches $|\mathbf{0}\rangle = |0\rangle^{\otimes N}$. As we discuss later, in practice, this can be hindered by the formation of dark states and the presence of different types of noise in the system.

In the following we shall perform exact and approximate numerical analysis to study this procedure. To quantify the level of lattice polarization, we define the average collective expectation value of the operators $\hat{S}^z$ as

$$\overline{S}_z = \frac{1}{N}\sum_{n=1}^{N} \frac{\langle \hat{S}_n^z \rangle}{s_n}, \quad (5)$$

with $\langle \hat{S}_n^z \rangle$ and s_n denoting the expectation value and spin number of the nth spin in the chain, respectively. In the current case we have $s_n = 1/2$. Note that the total polarization is normalized to unity and $-1 \leqslant \overline{S}_z \leqslant +1$. The exact numerics are performed by the QuTiP package [32]. Nonetheless, due to the limited computational power, the hyperpolarization of large spin systems is studied by a method based on the Holstein-Primakoff approximation, which is discussed next.

C. Gaussian states method

To study the behavior of large spin baths, we adopt a technique based on mapping the spin system onto a bosonic system, which, under a number of considerations discussed below, can then be numerically simulated with a significant computational advantage. To that end we make use of the Holstein-Primakoff transformation (HPT) and its corresponding approximation (HPA) and map Hamiltonian (3) onto a bosonic Hamiltonian [13,26]. In this method, a highly polarized spin is treated as a boson close to its ground state. It is worth mentioning that, despite this fact, in the hyperpolarization problem one usually takes the initial state of the spin bath in a fully thermal state. Nevertheless, since the state of the bath spins get closer to their respective ground state after each hyperpolarization cycle, the amount of total error committed in this method is tractable. Importantly, bosonic fields whose dynamics is ruled by Hamiltonians quadratic in the creation and annihilation operators preserve their Gaussian character at all times, provided that they are initialized in a Gaussian state. Given the fact that Gaussian states are completely characterized by their first and second moments, the equations of motion for those moments are enough to describe completely the system dynamics. Notably, those equations of motion have a dimensionality that grows linearly with the number of constituents, as opposed to the exponential growth of their Hilbert space. Therefore, simulating the evolution of the covariance matrix, which contains the second-order moments of the bosonic system, is enough to fully characterize the system dynamics and has considerably less complexity compared with the simulation of the time evolution of the density matrix.

Hamiltonian (3) can be exactly mapped onto bosons under the HPT. However, the resulting bosonic Hamiltonian is not quadratic in the creation and annihilation operators. This makes it difficult to study the system dynamics. One therefore takes its linear approximation, the lowest order of the HPA, that works the best for spin states that are close to their ground state. In this approximation, the spin operators of a spin-s particle are transformed as

$$\begin{aligned} \hat{s}^z &= \hat{a}^\dagger \hat{a} - s\mathbb{1}, \\ \hat{s}^+ &= \hat{a}^\dagger \sqrt{2s - \hat{a}^\dagger \hat{a}} \approx \hat{a}^\dagger \sqrt{2s}, \\ \hat{s}^- &= \sqrt{2s - \hat{a}^\dagger \hat{a}}\,\hat{a} \approx \sqrt{2s}\,\hat{a}, \end{aligned} \quad (6)$$

where $\hat{a}^\dagger$ ($\hat{a}$) is the bosonic creation (annihilation) operator with commutator $[\hat{a}, \hat{a}^\dagger] = \mathbb{1}$. Similarly, we perform the transformation for the Heisenberg chain operators by assigning the bosonic operators $\hat{b}_n$ who satisfy the commutation relation

$[\hat{b}_n, \hat{b}_m^\dagger] = \mathbb{1}\delta_{nm}$. By applying the above transformations the Hamiltonian in Eq. (3) reads

$$\hat{H}(t) = \omega_0 \hat{a}^\dagger \hat{a} + \frac{\lambda}{2}(\hat{b}_1^\dagger \hat{b}_1 + \hat{b}_N^\dagger \hat{b}_N) + (h-\lambda)\sum_{n=1}^{N} \hat{b}_n^\dagger \hat{b}_n + \lambda \sum_{n=1}^{N-1} \hat{b}_n^\dagger \hat{b}_{n+1} + \hat{b}_n \hat{b}_{n+1}^\dagger$$
$$+ \frac{1}{2}[\hat{b}_n^\dagger \hat{b}_n \overline{n}_{n+1}(t) + \hat{b}_{n+1}^\dagger \hat{b}_{n+1} \overline{n}_n(t)] + \sum_{n=1}^{N} J_n(\hat{a}^\dagger \hat{b}_n + \hat{a}\hat{b}_n^\dagger), \tag{7}$$

where to maintain the quadratic form of the Hamiltonian we have employed the mean-field approximation to deal with the terms arising from the $\hat{S}^z\hat{S}^z$ interactions. Here, $\overline{n}_i = \langle \hat{b}_i^\dagger \hat{b}_i \rangle$ is the instant occupation number of the ith spin site. The above Hamiltonian can be cast into the compact form of $\hat{H}(t) = \hat{\mathbf{R}}^\dagger V(t) \hat{\mathbf{R}}$ where we have introduced the bosonic operator vector $\hat{\mathbf{R}} = (\hat{a}, \hat{b}_1, \ldots, \hat{b}_N)^\mathsf{T}$ and the dynamical matrix:

$$V = \begin{pmatrix} \omega_0 & J_1 & J_2 & \cdots & J_N \\ J_1 & h + \frac{\lambda}{2}(\overline{n}_2 - 1) & \lambda & \cdots & 0 \\ J_2 & \lambda & h + \frac{\lambda}{2}(\overline{n}_1 + \overline{n}_3 - 2) & \cdots & 0 \\ \vdots & \vdots & \vdots & \ddots & \vdots \\ J_N & 0 & 0 & \cdots & h + \frac{\lambda}{2}(\overline{n}_{N-1} - 1) \end{pmatrix}.$$

This is an $(N+1)\times(N+1)$ matrix, where N is the total number of spins in the bath.

Since the initial spin bath state is assumed to be thermal and the control spin is put in the ground state, for the initial state one has $\langle \hat{\mathbf{R}} \rangle = 0$ and it retains this value given the purely quadratic form of Eq. (7). Starting from the von Neumann equation, it is straightforward to show that the evolution of the covariance matrix, $\Gamma_{i,j} = \langle \hat{R}_i^\dagger \hat{R}_j \rangle$, is given by

$$\dot{\Gamma} = -i[V(t), \Gamma], \tag{8}$$

whose formal solution is

$$\Gamma(t) = \mathcal{U}(t)\Gamma(0)\mathcal{U}^\dagger(t), \tag{9}$$

with $\mathcal{U}(t) = \exp[-i\int_0^t V(s)ds]$.

Furthermore, Eq. (5) can be expressed based on the bosonic operators

$$\overline{S}_z = \frac{1}{N}\sum_{n=1}^{N} \frac{\langle \hat{b}_n^\dagger \hat{b}_n \rangle - s_n}{s_n}. \tag{10}$$

We evaluate the hyperpolarization process by investigating the time evolution of $\overline{S}_z$ when the total initial state is set to $\rho(0) = |0\rangle\langle 0|_{\mathrm{cs}} \bigotimes_{n=1}^{N} \rho_n^{\mathrm{th}}$ and the system is subject to a series of polarization cycles as described in the previous section. We take $J_n = J/n^\alpha$ for the coupling of the control spin to the Heisenberg chain, without loss of generality. For $\alpha = 0$ the coupling is homogeneous, while other values of α represent a long-range coupling with various scalings. As $\alpha \to \infty$ one retrieves the nearest-neighbor coupling of the control spin to the spin at site $n = 1$. We first perform the numerical analysis with both exact and approximate methods for $N = 9$. The results are shown in Fig. 2(a). We compare the numerical outcomes of equations (5) and (10) that are referred to as exact and bosonic (HPA) approaches, respectively. In generating the plot we employ the following parameters: $\omega_0 = h = 100$, $\lambda = 2$, $J = 10$, and $\alpha = 2$. The polarization duration of each cycle is numerically optimized to $\tau = 5/h$. In fact, several different values of τ have been inspected, and that resulting in the greatest polarization transfer has been chosen. As can be seen, the exact (solid line) and the HPA (triangles) are well matched and approach to $\overline{S}_z = -1$. It is insightful to know how polarization of the individual spins evolves. Hence, we interrogate $\langle S_n^z \rangle / s_n$ for $n = 1, 5, 8$ and plot them in the inset of Fig. 2(a). The first spin in the chain (black line and stars) gets polarized quickly, as one would expect. Surprisingly, the fifth spin (magenta line and squares) is polarized slower than the eighth spin (green line and circles). We shall discuss about this behavior below. The agreement between the exact curves and HPA solutions implies that the HPA is valid in this system for the chosen set of parameters. This encourages us to extend this approximate method to larger spin systems where the simulation of the exact dynamics is numerically intractable.

In this spirit, we examine the polarization behavior for $N = 100$ based on the bosonic solution for the same system parameters. The solid blue line in Fig. 2(b) shows that the total polarization can reach values as high as $\overline{S}_z \approx -0.8$ after $R = 10\,000$ realizations. Higher amount of polarization is attainable for larger number of cycles, and thus, longer times. Moreover, while inspecting the individual spin polarizations we observe that the polarization of the spins at the beginning ($n = 1, \ldots, 7$) and at the end ($n = 96, \ldots, 100$) of the chain attain a larger amount of polarization compared with the rest of the spins. Meanwhile, the rate of polarizing is higher in the former group. This can be understood by considering the fact that these two groups have fewer neighbors from one of their ends. Yet, the first group ($n = 1, 2, \ldots, 7$) is closer to the control spin and polarizes faster. These can be seen from Fig. 2(b) where the polarizations of the third (green squares) and the 98th spin (red circles) are plotted as the representatives of the first and second groups, respectively. Moreover, the polarization of the 8th (magenta diamonds) and 95th (black stars) spins are also shown, revealing behavior of the "intermediate" spins.

We now analyze the efficiency of the hyperpolarization sequence as well as the accuracy of the approximate method employed in this work for various system parameters. In

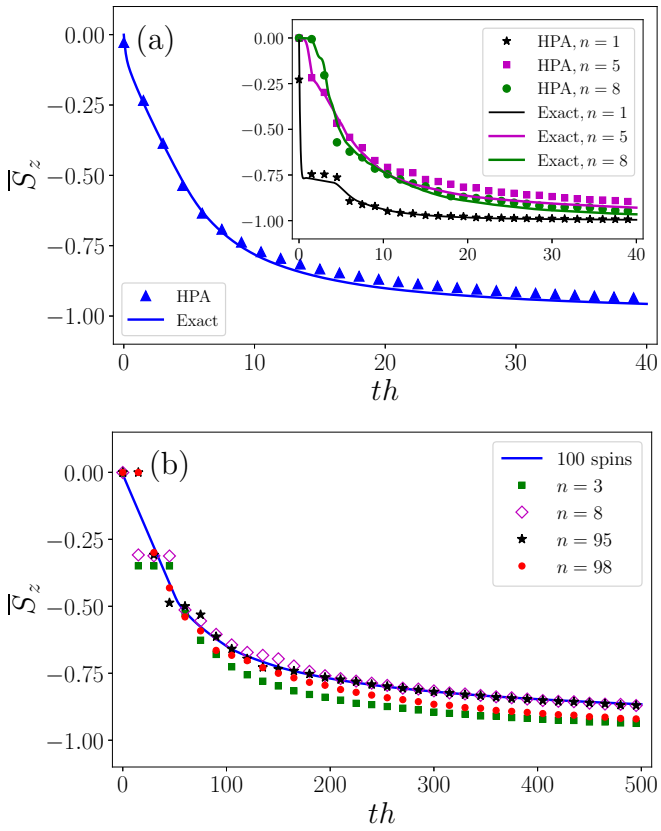

FIG. 2. The hyperpolarization dynamic of the Heisenberg model $\overline{S}_z$ as a function of the normalized polarization time th. (a) Comparison of the exact numerical simulation and HPA method for $N = 9$ spins with the polarization cycle time $\tau = 5/h$ and for $R = 800$. The inset in panel (a) displays the polarization dynamics of the individual spins. (b) The polarization dynamics for $N = 100$ based on the HPA approach with $R = 10\,000$. The parameters are $\omega_0 = h = 100$, $\lambda = 2, J = 10$, and $\alpha = 2$.

Fig. 3(a), we explore the role played by the strength of the spin interactions λ and J on the attainable hyperpolarization by simulating exactly a system with $N = 7$ and $\alpha = 2$. As can be observed, when λ is zero, which indicates that there is no interaction among spins within the chain, the hyperpolarization is negligible even for large values of J, that is, for strong couplings of the spins in the chain to the central spin. By increasing λ the polarization is improved and gets close to the maximum, $\overline{S}_z \approx -1$, for strong enough coupling rates to the central spin ($J > 5$). These show that the diffusion of polarization through interchain spin interactions is crucial for the hyperpolarization this one-dimensional lattice. A similar study is performed on the effect of the long-range interaction exponent, and reported in Fig. 3(c), where $\overline{S}_z$ is plotted against α for three different values of λ. For large enough interspin coupling rates larger values of α will favor the polarization. We compare these exact numerical results with the corresponding bosonic method by defining the relative error as $\varepsilon = ([\overline{S}_z]_{\text{exact}} - [\overline{S}_z]_{\text{HPA}})/|[\overline{S}_z]_{\text{exact}} + [\overline{S}_z]_{\text{HPA}}|$, which assumes both positive (overestimating the exact results) and negative (underestimating the exact results) values. The relative error behavior is shown in Fig. 3(b) where the dotted area identifies parameter region where the difference between the exact and the bosonic methods is less than 1%, while the hashed area corresponds to the parameter region where the HPA method underestimates the exact results with less than a 5% error. Note that our goal is to find the parameters that both give a high polarization and low relative error. Hence, the highest polarization associated with the least relative error can be generally obtained for $J \geqslant 10$ and $\lambda \geqslant 2$. These two optimal limits also explain our choice of parameters in Fig. 2. A similar study is performed for α and it is found that the relative error saturates and becomes less that one percent for $\alpha \geqslant 2$, see Fig. 3(d).

This concludes our introduction to the possibility of hyperpolarization by an optically active spin in a simple one-dimensional lattice and the analysis of the validity of bosonic model. In the next section we consider the same problem for a real two-dimensional hexagonal boron nitride (hBN) lattice with an optically active color center.

III. HEXAGONAL BORON NITRIDE LATTICE

Hexagonal boron nitride is an ideal van der Waals crystal for hosting optically active defects since it has a large band gap (≈6 eV) [18,33]. Defects in hBN can be exploited for flexible two-dimensional quantum sensors [34,35]. Furthermore, there are proposals for employing the freestanding layers of hBN as optomechanical systems [36,37], which are based on the exceptional mechanical properties of the hBN and the accompanying color centers [38].

Each site in the hBN lattice is occupied by either a nitrogen atom or a boron atom, both of which have a nonzero nuclear spin. A schematic of the hBN lattice with a V_B defect is shown in Fig. 1(b) consisting of a missing boron atom. The negatively charged boron vacancy center has a triplet spin ground state ($S = 1$) with zero-field splitting $D/2\pi \approx 3.5$ GHz, which can be efficiently polarized optically [39]. Moreover, transitions among the ground-state levels can be induced through suitable microwave drives. The simplified energy-level diagram of the V_B defect is depicted in Fig. 1(c). In fact, the defect radiates a red light at a wavelength centered at ≈850 nm when excited with a green 532 nm laser. In the following sections we introduce the nuclear spin bath model and then study the possibility of hyperpolarizing the hBN spin lattice. For the sake of simplicity, we shall assume that the sample is purified to the ^{11}B isotopes.

A. The nuclear spin bath model

The hyper-fine (hf) interaction between the color center and a nucleus is produced by two mechanisms of different physical origin and which can both contribute to the coupling between an electron spin $\mathbf{S}$ and a nuclear spin $\mathbf{I}$. The first mechanism is the magnetic dipole-dipole interaction between the magnetic moments of the electron and nuclear spins. In analogy to the classical dipolar interaction between magnetic moments its Hamiltonian is written as

$$\hat{H}_{\text{dd}}^{e,i} = \frac{\mu_0}{4\pi}\frac{\gamma_e \gamma_{n,i}}{r_i^3}\left[\hat{\mathbf{S}}\cdot\hat{\mathbf{I}}_i - \frac{3(\hat{\mathbf{S}}\cdot\mathbf{r}_i)(\hat{\mathbf{I}}_i\cdot\mathbf{r}_i)}{r_i^2}\right], \qquad (11)$$

where μ_0 is the permeability of the vacuum and $\mathbf{r}_i$ is the displacement vector pointing from electron to the ith nucleus (in

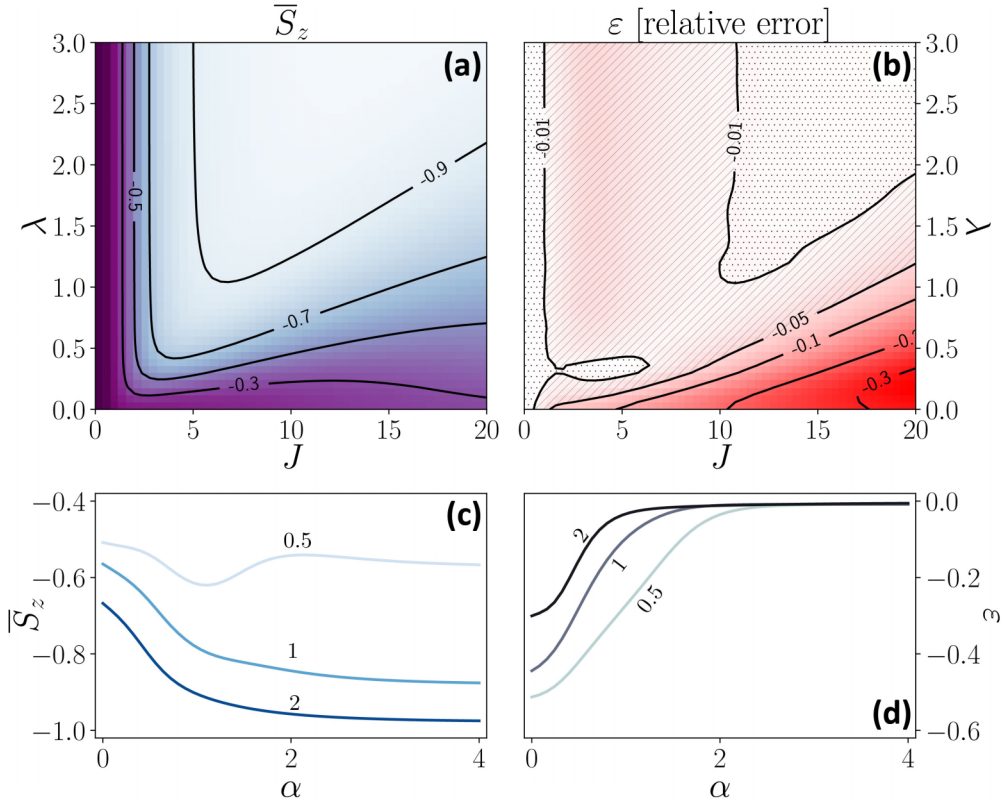

FIG. 3. The exact numerical simulation of hyperpolarization in the central spin model and its comparison to the Gaussian method: (a) The exact polarization and (b) the relative error of the corresponding Gaussian simulation ε as a function of J and λ for $\alpha = 2$. (c) Variations of the polarization and (d) the relative error ε as functions of the coupling exponent α for $J = 10$. The numbers next to each line correspond to a different value of λ. The other parameters are $\omega_0 = h = 100$, $\tau = 5/h$, $N = 7$, and $R = 500$.

meters) and $\hat{\mathbf{r}}_i$ is the corresponding unit vector. Here, γ_e and $\gamma_{n,i}$ are the gyromagnetic ratios of the electron and nucleus at site i, respectively. The dipole-dipole interaction depends on the relative orientation of the magnetic moments and is thus anisotropic. A purely dipolar interaction is expected if the electron spin is located in a molecular orbital with no overlap with the nuclei. In contrast, the second hf mechanism becomes important if there is a finite probability of the electron presence at the location of the nuclei. In fact, this is the case only if there are contributions of $1s$ orbital (totally symmetric orbital) to the molecular orbitals that accommodate the electron of interest [2,40]. The energy term of this so-called Fermi contact interaction is given by

$$\hat{H}_{\mathrm{Fc}} = \frac{8\pi}{3}\frac{\mu_0}{4\pi}\gamma_e \sum_i \gamma_{n,i}|\Psi(\mathbf{r}_i)|^2 \hat{\mathbf{S}}\cdot\hat{\mathbf{I}}_i. \tag{12}$$

Here, $|\Psi(\mathbf{r}_i)|^2$ is the probability density of the electron in the orbital described by the wave function Ψ. Evidently, the Fermi contact interaction is isotropic.

In the ground state of the negatively charged boron vacancy the electrons occupy well-localized molecular orbitals, which have little overlap with the lattice nuclei [23,41]. Hence, the dipole interaction is the dominant term when the polarization of a large spin lattice is concerned.

We now study the hyperpolarization of a monolayer of hexagonal boron nitride lattice by the electron spin of the V_B defect. We consider the nuclear-spin lattice of a monolayer of hBN of arbitrary size. We assume an isotope purified sample and only take into account the naturally prominent isotope of boron, that is, ^{11}B, whose natural abundance is around 80 percent. The nuclear spins of the different constituents of the lattice are the following:

$$S_{\mathrm{V_B}} = 1, \quad S_{\mathrm{N}} = 1, \quad S_{\mathrm{B}} = 3/2. \tag{13}$$

Here, we study a protocol that can acquire rapid hyperpolarization of both nitrogen and boron nuclear spins at room temperature, starting from thermal distributions. The electron spin of the V_B defect is first polarized with a short laser pulse. Then the polarization is transferred to the nuclei through their hyperfine interaction, where resonance is achieved by suitably driving the ground state of the color center with a microwave field. This is optimal when the Hartmann-Hahn resonance is satisfied. The process is repeated by polarizing the electron spin and continues as many times as necessary to arrive at the highest polarization level. Note that even in ideal conditions one cycle of the polarization transfer is not enough for polarizing one single nuclear spin (boron or nitrogen). Because the spin of nuclear spins is higher than that of the effective one-half spin of the defect, see below. Therefore, to obtain a strong polarization, it is requisite to exploit many reiterations of the polarization protocol.

Meanwhile, the nuclear spins are coupled to each other via the dipole-dipole interactions:

$$\hat{H}^{ij}_{\mathrm{dd}} = \hbar g_{ij}[\hat{\mathbf{I}}_i\cdot\hat{\mathbf{I}}_j - 3(\hat{\mathbf{I}}_i\cdot\hat{\boldsymbol{r}}_{ij})(\hat{\mathbf{I}}_j\cdot\hat{\boldsymbol{r}}_{ij})], \tag{14}$$

where $g_{ij} = \hbar\mu_0\gamma_{n,i}\gamma_{n,j}/4\pi|\mathbf{r}_{ij}|^3$ is the coupling strength and $\hat{\mathbf{I}}_i = (\hat{I}_i^x, \hat{I}_i^y, \hat{I}_i^z)$ is the vector of spin operators. Here, $\mathbf{r}_{ij} = \mathbf{r}_i - \mathbf{r}_j$ is the spatial vector connecting the two interacting spins, with $\hat{\boldsymbol{r}}_{ij} = (\hat{x}_{ij}, \hat{y}_{ij}, \hat{z}_{ij})$ its corresponding unit vector. The lattice constant in hBN is ≈1.5 Å, while the boron and nitrogen gyromagnetic ratios are $\gamma_B/2\pi = 13.66$ MHz/T and $\gamma_N/2\pi = 3.078$ MHz/T, respectively. As shall become clear in the next section, unlike the simple one-dimensional Heisenberg chain these internuclei interactions do not contribute to the hyperpolarization process; in contrast, they can be detrimental.

B. Engineering the system dynamics

We take into account N symmetrically nearest nuclear spins to the defect and assume a high external magnetic field such that $D \ll \gamma_e|\mathbf{B}|$, see the inset in Fig. 1(c). In this configuration, the defect natural quantization axis is suppressed and the magnetic field orientation dictates the quantization axis for both electron and nuclei, which we assign to the z axis. By applying a microwave field driving the transition $|-1\rangle \leftrightarrow |0\rangle$ with Rabi frequency Ω and under the rotating wave approximation, the total effective Hamiltonian describing the dynamics of the system in the frame rotating with the driving field frequency $\omega_{\rm mw}$ reads

$$\hat{H}_{\rm eff} = \Omega\hat{s}^z + \sum_{i=1}^{N}\acute{\omega}_i\hat{I}_i^z + \sum_{i=1}^{N}(\alpha_i\hat{s}^+\hat{I}_i^- + \alpha_i^*\hat{s}^-\hat{I}_i^+) + \sum_{i<j}^{N} b_{ij}\left(\hat{I}_i^z\hat{I}_j^z - \frac{1}{4}(\hat{I}_i^+\hat{I}_j^- + \hat{I}_i^-\hat{I}_j^+)\right), \tag{15}$$

where $\hat{s}^z = \frac{1}{2}(|+\rangle\langle+| - |-\rangle\langle-|)$ and $\hat{s}^+ = |+\rangle\langle-| = (\hat{s}^-)^\dagger$ are the Pauli matrices in the dressed state basis $|\pm\rangle = (|0\rangle \pm |-1\rangle)/\sqrt{2}$ representation, see the Appendix for details of the derivation. Here, the hyperfine coupling $\alpha_i = \frac{1}{4}(A_i^x + iA_i^y)$, the modified nuclear Larmor frequencies $\acute{\omega}_i = \omega_i - \frac{1}{2}A_i^z$, and the internuclei dipolar coupling rate $b_{ij} = g_{ij}(1 - 3\hat{z}_{ij}^2)$ have been introduced. The hyperfine coupling vector of the electron spin to the ith nuclear spin is given by $\mathbf{A}_i = g_{ei}(-3\hat{x}_i\hat{z}_i, -3\hat{y}_i\hat{z}_i, 1 - 3\hat{z}_i^2)$ with $g_{ei} = \hbar\mu_0\gamma_e\gamma_{n,i}/(4\pi|\mathbf{r}_i|^3)$.

It is clear from the above Hamiltonian and the hyperfine vector that hyperpolarization of a monolayer of hBN is not possible when the quantization axis is perpendicular to the layer, whenever the conditions for the rotating wave approximation are satisfied. Because in this case $\alpha_i = 0$, and thus, the flip-flop interactions between the defect and the nuclear spins cannot occur. To circumvent this, we assume that a high magnetic field, tilted with respect to the layer, is applied with a deviation angle θ, see Fig. 1(b) for the sketch. Note that, in the limit of weak magnetic field, the natural quantization axis of V_B in its D_{3h} symmetry is perpendicular to the layer, and thus, the hyperpolarization is inaccessible. This also explains our choice of large magnetic field at the beginning of this section.

Note that for magnetic fields where the electronic- and nuclear-spin transitions become resonant; that is, close to the ground-state level anticrossing (GSLAC), in-plane flip-flop interactions become allowed. The above assumption about magnetic field direction is not correct in general, but it is valid for our configuration with the RWA.

We next find the angle θ that maximizes the flip-flop interactions responsible for the polarization transfer. It is straightforward to obtain

$$|\alpha_i| = \tfrac{1}{4}\sqrt{|A_i^x|^2 + |A_i^y|^2} = \tfrac{3}{8}g_{ei}|\sin(2\theta)|. \tag{16}$$

Therefore, the greatest amount of $|\alpha_i|$ is found for $\theta = \frac{\pi}{4}$. Nonetheless, the azimuthal angle of the magnetic field also plays an important role here and can be employed for tuning the coupling of the defect to different sites. We find the optimal azimuthal angle numerically.

C. Hyperpolarization of hexagonal boron nitride

The hyperpolarization scheme is similar to the one explained in Sec. II B and can be summarized as follows: First, by using an optical pumping the electron spin of the ground state of the V_B defect is brought to the $|0\rangle$, i.e., the state with $m_s = 0$. Then it is prepared in the superposition state $|-\rangle = (|0\rangle - |-1\rangle)/\sqrt{2}$ by applying a $\frac{\pi}{2}$ pulse [39]. Second, the polarization is transferred from the V_B spin to the nuclear spins via the hyperfine interactions, which are made resonant by applying a suitable resonant microwave drive. The steps of the polarization cycle are iterated multiple times. Nonetheless, one should keep in mind that since there are two spin species (three for the natural isotope shares) in the lattice, the resonance condition cannot simultaneously hold for all the spins in the bath. Given the long coherence time of the nuclear spins this can be circumvented, e.g., by alternating the resonant condition for all spin species of interest. The whole initial state is $\rho(0) = \rho_e(0)\bigotimes_{i=1}^{N}\rho_i^{\rm th}$ where the initial state of the defect is set to $\rho_e(0) = |-\rangle\langle-|$. Meanwhile, the nuclear spins are assumed to be in thermal equilibrium with independent reservoirs, and thus, their initial density matrix is given by $\rho_i^{\rm th}$. The evolution of the nuclear-spin density matrix after the $(R+1)$st cycle of the polarization protocol is determined by

$$\hat{\rho}_{\rm nuc}((R+1)\tau) = {\rm Tr}_e\{e^{-i\hat{H}_{\rm eff}\tau}[|-\rangle\langle-|_e \otimes \hat{\rho}_{\rm nuc}(R\tau)]e^{i\hat{H}_{\rm eff}\tau}\}, \tag{17}$$

where $\hat{H}_{\rm eff}$ is the Hamiltonian (15), τ is the equal duration of each cycle, and ${\rm Tr}_e\{\}$ denotes the trace over the electron spin.

To numerically simulate a large spin system we shall employ the method based on HPA explained and examined in the previous section. Under this transformation, i.e., Eq. (6), and for resonant driving of the electron, the Hamiltonian (15) takes the following form:

$$\hat{H}(t) = \Omega\,\hat{a}^\dagger\hat{a} + \sum_{i=1}^{N}\tilde{\omega}_i(t)\,\hat{b}_i^\dagger\hat{b}_i + \sum_{i=1}^{N}(\beta_i\hat{a}^\dagger\hat{b}_i + \beta_i^*\hat{a}\hat{b}_i^\dagger) - \sum_{i<j}^{N}B_{ij}(\hat{b}_i^\dagger\hat{b}_j + \hat{b}_i\hat{b}_j^\dagger), \tag{18}$$

where we have introduced the electron-nuclei coupling rate $\beta_i = \sqrt{2s_i}\alpha_i$ and nuclear-nuclear interaction strengths $B_{ij} = \frac{1}{2}\sqrt{s_is_j}\,b_{ij}$. Here, the modified Larmor frequency of the nuclear spins is $\tilde{\omega}_i(t) = \acute{\omega}_i + \frac{1}{2}\sum_{j\neq i}b_{ij}(\overline{n}_j(t) - 2s_j)$ where the time-dependent expectation value is due to the mean-field

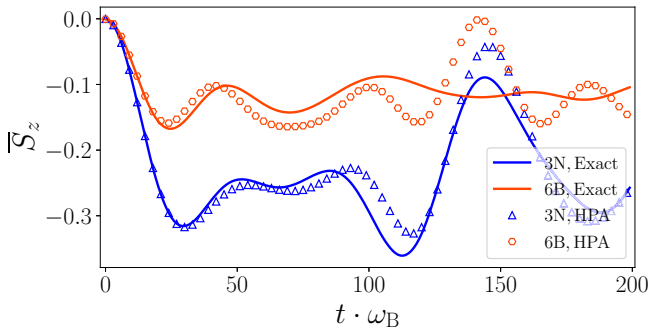

FIG. 4. The short time polarization dynamics of the defect and the nearest nuclei: $\overline{S}_z$ is given separately for the three nitrogens (blue) and six borons (red) which are the nearest nuclei to the V_B. The exact results are shown by solid lines, while those computed through the HPA method are given as markers. The V_B and the nuclei states are initially set to $|-\rangle$ and a fully thermal state, respectively. The magnetic field is $B = 1$ T and the Rabi frequencies are set to satisfy the Hartmann-Hahn resonance conditions.

approximation. This Hamiltonian is quadratic in the bosonic operators, and this allows for an efficient and tractable numerical simulation describing the dynamical evolution via the covariance matrix formalism. The above Hamiltonian according to the bosonic operator vector $\hat{\mathbf{R}} = (\hat{a}, \hat{b}_1, \ldots, \hat{b}_N)^{\mathsf{T}}$ can be expressed as $\hat{H}(t) = \hat{\mathbf{R}}^{\dagger} W(t) \hat{\mathbf{R}}$, with the dynamics matrix

$$W(t) = \begin{pmatrix} \Omega & \beta_1 & \beta_2 & \beta_3 & \cdots & \beta_N \\ \beta_1^* & \tilde{\omega}_1(t) & -B_{12} & -B_{13} & \cdots & -B_{1N} \\ \beta_2^* & -B_{12} & \tilde{\omega}_2(t) & -B_{23} & \cdots & -B_{2N} \\ \beta_3^* & -B_{13} & -B_{23} & \tilde{\omega}_3(t) & \cdots & -B_{3N} \\ \vdots & \vdots & \vdots & \vdots & \ddots & \vdots \\ \beta_N^* & -B_{1N} & -B_{2N} & -B_{3N} & \cdots & \tilde{\omega}_N(t) \end{pmatrix}.$$

Thanks to the quadratic form of the Hamiltonian (18) the system is fully characterized by the first and the second moments of the operators $\hat{\mathbf{R}}$. The covariance matrix, $\Gamma_{i,j} = \langle \hat{R}_i^{\dagger} \hat{R}_j \rangle$, is sufficient for describing the system dynamics when the initial state gives zero-mean value. In our case, the nuclei are initially set to a thermal state and the electron is in the ground state of the dressed state basis. Therefore, we have $\langle \hat{\mathbf{R}} \rangle = 0$ and proceed with analyzing the covariance matrix dynamics by employing Eq. (9).

Before studying large-size systems, we compare the HPA technique and the exact numerical simulation for first two rings: Three nearest nitrogen nuclei and six next-nearest boron nuclei, see Fig. 1(b) for a graphical illustration. To this end, we investigate the short-time dynamics, where the nuclear spins are all taken to be spin 1/2 systems and their couplings vary according to equations (15) and (18) depending on whether they represent a boron or a nitrogen nuclear spin. In Fig. 4 the results are compared when the nuclei are initially set to the thermal state while the defect electron spin is initialized in the dressed state of $|-\rangle$. The solid curves in Fig. 4 show the numerical simulation of Hamiltonian (15). We notice that the HPA method captures most features of the exact numerics despite the thermal initial state of the nuclei. This is such that the

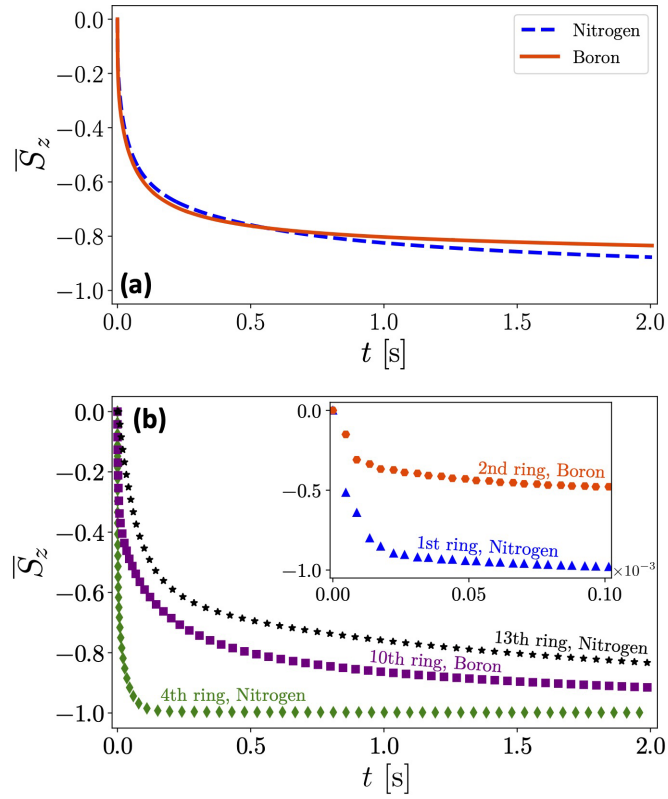

FIG. 5. Hyperpolarization of hBN lattice: (a) The polarization dynamics is represented for 121 nuclei spins composed of 61 nitrogens and 60 borons with $R = 15 \times 10^5$. (b) The polarization behavior for five different rings. The inset gives the polarization evolution of the two first rings after $R = 70$. The other parameters are $\tau_N = 25/\omega_N$, $\tau_B = 15/\omega_B$, and $B = 1$ T.

results even show perfect match for $t \lesssim 25/\omega_B$. However, for longer timescales, the approximate methods deviate from the exact numerics as the incurred errors build up. The deviations grow larger as the time elapses and the HPA method becomes less reliable. Therefore, in our following hyperpolarization study for large systems, which is based on the HPA method, we always choose $\tau < 25/\omega_B$ to ensure the validity of the results.

In the hyperpolarization procedure, we take the combination of two different Rabi frequencies that each satisfy the Hartmann-Hahn resonance condition for the boron and nitrogen nuclei. This is to guarantee the polarization of both sublattices. In other words, we set $\Omega = \omega_N$ and $\Omega = \omega_B$ alternating in the polarization cycle iterations. The duration of polarization for each step is numerically optimized to $\tau_N = 25/\omega_B$ and $\tau_B = 15/\omega_B$. That is, many different values of τ_N and τ_B have been investigated and these are found to be the values that result in the highest polarization in the shortest time.

Now, we extend our analysis based on the HPA method to the largest spin system that our computational resources can afford. Hence, we assume a spin lattice with $N = 121$ composed on 61 nitrogen and 60 boron spins. The results are provided in Fig. 5(a), where one observes a smooth trend in the average polarization of both boron and nitrogen

sublattices. Nevertheless, there is a slight difference in their behavior. The borons polarize slightly faster due to their stronger interaction with the defect electron spin. But their polarization already saturates after $R = 15\times10^5$ cycles. We attribute this to the larger coupling rate among the boron nuclei, which in turn stems from their larger gyromagnetic ratio. On the other hand, the nitrogen sublattice polarizes with a slower pace, yet it has the potential of approaching higher values of polarization over longer times. Our findings suggest that—unlike the one-dimensional case—in two-dimensional (and presumably higher-dimensional) lattices the strong interaction among the spins in the bath can hinder the polarization transfer; see the discussion at the end of this section.

To better understand the dynamics of the system we also examine the polarization process of sets of nuclei that are equidistant to the V_B. We refer to each of these sets as the "rings" around the defects. This is such that the three nearest-neighbor nitrogens lie in the first ring, the second ring is composed of six borons in the next-nearest neighbor, and so on as follows: Three nitrogens in the third ring, six nitrogens in the fourth ring, six borons in the fifth ring. Figure 5(b) shows the polarization for some of the rings. The first and second rings already get polarized to their asymptotic value after $R \approx 70$. This rapid polarization of these two rings is understandable because of their proximity to the defect. For the three nitrogen nuclei the weak interaction among themselves allows for a perfect polarization. Meanwhile, the fast but limited polarization ($\overline{S}_z \approx -0.5$) of the second ring is ascribed to the competition between the internuclei and defect-nuclei interactions. However, for rings farther from the defect, the distance among borons increases and consequently the internuclei interactions become much weaker. Hence, the boron spins in the tenth ring continue their journey to the ground state, although very slowly, see the purple squares in the leftmost part of the plot. The trend is more or less the same for farther rings of both species. Note that the tenth and thirteenth rings have 12 borons and 12 nitrogens, respectively.

To further assess the effect of internuclei interactions on the polarization transfer from the V_B defect to the spins bath, we *artificially* turn off the defect-nuclei interactions in three different scenarios: We first suppose that only the nitrogen spins interact with the defect, while the borons are decoupled from it. However, we allow them to interact among each other as well as with the nitrogen spins. Next, we perform the same study by swapping the role of boron and nitrogen. In another scenario, we allow the defect to only interact with the first and second ring nuclei, while the rest of lattice does not have any direct interaction with the defect. In all these investigations we generally find that the interaction between the nuclei is not able to transfer the polarization from one species to another or even from closer rings to the farther nuclei.

Notice that internuclear interactions can hinder the polarization transfer in several ways. The build up of coherences between nuclear spins can generate "dark states," which lead to a decoupling of the color center from the nuclear spin ensemble and thus the transfer of polarization from the color center to the nuclear spin lattice is inhibited [42]. Therefore, for the polarization of regions within the neighborhood of the color center, internuclear couplings are, in general, not desirable. However, to polarize regions far from the color center, one needs to rely on the diffusion of polarization via the internuclear interaction. In this case, it is the internuclear interaction terms of the form $\hat{I}_i^z\hat{I}_j^z$ which can become detrimental. In particular, such a term can bring neighboring nuclei out of resonance, when each see environments with a different degree of polarization. This loss of resonance in turn will degrade the internuclear coupling and hinder the diffusion of polarization.

Finally, note that, in practice, the polarization saturation levels will depend on the rates of dissipative processes. One can consider at least three ways in which the action of the environment on the system can affect the achieved polarization. (i) The exact polarization rates and saturation levels could deviate from the ideal case studied here if the coherence times of both the color center and the nuclear spins fall below the duration of a single polarization cycle. (ii) The polarization of the nuclear spins can be lost through spin relaxation processes, typically resulting from the interaction of the nuclei with lattice phonons. Thus, the final saturation levels of the polarization will depend on the ratio between the polarization rate and the relaxation rate of the nuclear spins. (iii) Notably, not all sources of noise are detrimental for the polarization of the nuclear spin lattice and in some cases the presence of dephasing noise can indeed give rise to better polarization. The dephasing noise, e.g., from a fluctuating magnetic field, leads to the destruction of coherences among nuclear spins. Hence the dark states are destroyed, which in turn leads to higher saturation levels of the polarization [43]. A more precise benchmark of the performance of our protocol in the presence of these sources of noise requires a proper quantum open-system analysis together with its corresponding numerical simulation, which is out of scope of the current work and will be presented elsewhere.

IV. CONCLUSION

We have presented a theoretical description of the efficient polarization transfer from a V_B defect to the nuclear spins in the hexagonal boron nitride lattice at room temperature by manipulating an optically active electron spin. Since a large spin system cannot be simulated by exact methods, we have studied the hyperpolarization via a numerical method based on the Holstein-Primakoff approximation. By considering the central spin model as a well-understood system, we have benchmarked the method and have found that the HPA numerical approach is in good agreement with exact numerical simulation and yields satisfactory results. This has allowed us to design and optimize numerically a polarization sequence that may be implemented experimentally to reach large levels of nuclear spin polarization in hBN. Our results pave the way for the utilization of defects in hexagonal boron nitride for quantum technologies, and high-resolution two-dimensional quantum sensors such as NMR.

ACKNOWLEDGMENTS

F.T.T. and M.F. acknowledge the support by Iran Science Elites Federation via a postdoctoral fellowship. The work of J.S.P. and M.B.P. was supported by ERC HyperQ.

APPENDIX A: DERIVATION OF THE EFFECTIVE HAMILTONIAN (15)

In this Appendix we provide the detailed steps in arriving to the effective Hamiltonian (15) employed for studying the hyperpolarization of hBN nuclear-spin lattice. We begin by considering an external magnetic field which defines the z axis of the laboratory frame of reference and assume a hBN layer that the V_B defect is located at the origin. It should be noted that V_B has a D_{3h} symmetry with the axis of symmetry perpendicular to the layer such that the misalignment angle between the magnetic field and V_B axis is given by θ, see Fig. 1(b). We suppose the applied magnetic field is strong, $D \ll \gamma_e|\mathbf{B}|$, such that the quantization axis is determined by the magnetic field and the zero-field splitting will be regarded as a perturbation that leads to energy shifts of the Hamiltonian diagonal elements [16,44]. The total Hamiltonian describing dynamics of the system in the laboratory frame reads $\hat{H} = \hat{H}_0 + \hat{H}_I$, where $\hat{H}_0$ constitutes the V_B defect and the nuclear spin lattice free Hamiltonians:

$$\hat{H}_0 = [\omega_e + \delta(\theta)]\hat{S}_z + D(\theta)\hat{S}_z^2 + \sum_{i=1}^{N} \omega_i \hat{I}_i^z, \tag{A1}$$

where $\omega_e = -\gamma_e B$ and $\omega_i = \gamma_{n,i} B$ are, respectively, the Larmor frequencies of electron and the nuclei, and we have introduced

$$D(\theta) = \frac{D}{4}(1 + 3\cos 2\theta),$$
$$\delta(\theta) = \frac{D^2}{8\omega_e}\left[\sin^4\theta + \frac{\sin^2(2\theta)}{1 - (D(\theta)/\omega_e)^2}\right],$$

where D denotes the zero-field splitting of the defect [16].

The interaction Hamiltonian is given by

$$\hat{H}_I = \sum_{i=1}^{N} \hat{H}_{\rm dd}^{e,i} + \sum_{i<j}^{N} \hat{H}_{\rm dd}^{ij}. \tag{A2}$$

Before proceeding, we simplify the interactions by applying the secular approximation. For this purpose we first express the interactions in terms of the spin raising and lowering operators $\hat{I}_i^{\pm} = \hat{I}_i^x \pm i\hat{I}_i^y$. Hence, Eq. (14) becomes

$$\hat{H}_{\rm dd}^{ij} = b_{ij}\left[\hat{I}_i^z\hat{I}_j^z - \tfrac{1}{4}(\hat{I}_i^+\hat{I}_j^- + \hat{I}_i^-\hat{I}_j^+)\right] + \left[c_{ij}\left(\hat{I}_i^z\hat{I}_j^+ + \hat{I}_i^+\hat{I}_j^z\right) + d_{ij}(\hat{I}_i^+\hat{I}_j^+) + \text{H.c.}\right], \tag{A3}$$

where have introduced the following coefficients:

$$b_{ij} = g_{ij}\left(1 - 3\hat{z}_{ij}^2\right),$$
$$c_{ij} = -\tfrac{3}{2}g_{ij}(\hat{x}_{ij} - i\,\hat{y}_{ij})\hat{z}_{ij},$$
$$d_{ij} = -\tfrac{3}{4}g_{ij}\left(\hat{x}_{ij}^2 - \hat{y}_{ij}^2 - 2i\hat{x}_{ij}\hat{y}_{ij}\right).$$

In the interaction picture of the free nuclear-spin lattice Hamiltonian, the nuclear spins transform as

$$\hat{I}_i^{\pm} \to \hat{I}_i^{\pm} e^{\pm i\omega_i t}, \quad \hat{I}_i^z \to \hat{I}_i^z. \tag{A4}$$

Under the rotating wave approximation, which is valid if the applied magnetic field is high, and thus, the Larmor frequencies are much larger than the dipole-dipole coupling, i.e., $\{\omega_i, \omega_j\} \gg g_{ij}$, one neglects the effect of the resulting time-dependent terms in Eq. (A3). Hence, the spin-spin interaction reduces to

$$H_{\rm dd}^{ij} \approx b_{ij}\left[\hat{I}_i^z\hat{I}_j^z - \tfrac{1}{4}(\hat{I}_i^+\hat{I}_j^- + \hat{I}_i^-\hat{I}_j^+)\right]. \tag{A5}$$

For the interaction of the defect electron spin with the nuclear spins, which have gyromagnetic ratios differing by about three orders of magnitude, one has

$$\hat{H}_{\rm dd}^{ei} \approx \hat{S}_z\,\mathbf{A}_i \cdot \hat{\mathbf{I}}_i, \tag{A6}$$

where $\mathbf{A}_i = g_{ei}(-3\hat{x}_i\hat{z}_i, -3\hat{y}_i\hat{z}_i, 1 - 3\hat{z}_i^2)$ with $g_{ei} = \hbar\mu_0\gamma_e\gamma_{n,i}/4\pi|\mathbf{r}_i|^3$ is the hyperfine coupling vector of the electron spin to the ith nuclear spin. Note that we have simplified the hyperfine interaction by secular approximation, since the nonsecular hyperfine coupling can be neglected at magnetic fields that provide large differences between the electronic and nuclear Zeeman splitting, i.e., $|\omega_e + \delta(\theta) - \omega_i| \gg g_{ei}$. Hence, after applying the secular approximations the Hamiltonian describing the system dynamics reads

$$\hat{H} = [\omega_e + \delta(\theta)]\hat{S}_z + D(\theta)\hat{S}_z^2 + \sum_{i=1}^{N}\omega_i\hat{I}_i^z + \sum_{i=1}^{N}\hat{S}_z\,\mathbf{A}_i\cdot\hat{\mathbf{I}}_i + \sum_{i<j}^{N} b_{ij}\left(\hat{I}_i^z\hat{I}_j^z - \frac{1}{4}(\hat{I}_i^+\hat{I}_j^- + \hat{I}_i^-\hat{I}_j^+)\right). \tag{A7}$$

The flip-flop interaction of the electron spin with the nuclei—necessary for polarization transfer—is negligible as $\omega_e \gg \omega_i$. Nevertheless, an efficient two-level system that is on resonance with the bath spins is constructed by a microwave drive with a proper frequency and amplitude. In our analysis we assume that the microwave field applied to the V_B defect is tuned for driving the spin transition $|0\rangle \leftrightarrow |-1\rangle$. The corresponding Hamiltonian is then

$$\hat{H}_{\rm mw} = \Omega(|0\rangle\langle -1|\, e^{-i\omega_{\rm mw}t} + |-1\rangle\langle 0|\, e^{i\omega_{\rm mw}t}), \tag{A8}$$

where Ω is the Rabi frequency and $\omega_{\rm mw}$ is the frequency of the driving field. We add $\hat{H}_{\rm mw}$ to the Hamiltonian in Eq. (A7) and move to the frame rotating at $\omega_{\rm mw}$ to arrive at

$$\hat{H} = \Delta\tilde{s}^z + \Omega\tilde{s}^x + \sum_{i=1}^{N}\omega_i\hat{I}_i^z + \sum_{i=1}^{N}\left(\tilde{s}^z - \frac{1}{2}\mathbb{1}\right)\mathbf{A}_i\cdot\hat{\mathbf{I}}_i + \sum_{i<j}^{N} b_{ij}\left(\hat{I}_i^z\hat{I}_j^z - \frac{1}{4}(\hat{I}_i^+\hat{I}_j^- + \hat{I}_i^-\hat{I}_j^+)\right), \tag{A9}$$

where $\Delta = \omega_e + \delta(\theta) - D(\theta) - \omega_{\rm mw}$ is the detuning and we have dropped the contribution from $|+1\rangle$ in the electron-spin dynamics justified through the rotating wave approximation. We, thus, have introduced the two-level electron-spin operators $\tilde{s}^z = \frac{1}{2}(|0\rangle\langle 0| - |-1\rangle\langle -1|)$ and $\tilde{s}^x = \frac{1}{2}(|0\rangle\langle -1| + |-1\rangle\langle 0|)$ in the subspace spanned by states $\{|0\rangle, |-1\rangle\}$.

In the dressed state basis $|\pm\rangle = (|0\rangle \pm |-1\rangle)/\sqrt{2}$ representation and neglecting the fast oscillating terms, the

Hamiltonian (A9) reads

$$\hat{H}_{\text{eff}} = \Delta\hat{s}^x + \Omega\hat{s}^z + \sum_{i=1}^{N}\acute{\omega}_i\hat{I}_i^z + \sum_{i=1}^{N}(\alpha_i\hat{s}^+\hat{I}_i^- + \alpha_i^*\hat{s}^-\hat{I}_i^+) + \sum_{i<j}^{N} b_{ij}\left(\hat{I}_i^z\hat{I}_j^z - \frac{1}{4}(\hat{I}_i^+\hat{I}_j^- + \hat{I}_i^-\hat{I}_j^+)\right), \tag{A10}$$

where $\{\hat{s}^z, \hat{s}^x, \hat{s}^\pm\}$ are the Pauli matrices in the dressed basis representation. Here, the hyperfine coupling $\alpha_i = \frac{1}{4}(A_i^x + iA_i^y)$ and the modified nuclear Larmor frequencies $\acute{\omega}_i = \omega_i - \frac{1}{2}A_i^z$ have been introduced. Note that this last secular approximation is justified when $\{\Omega, \omega_i\} \gg g_{ei}$, which can be attained by operating the system at high magnetic fields. In this work we assume $\Delta = 0$, which is suited for the polarization transfer, and arrive to the effective Hamiltonian Eq. (15).

[1] A. M. Stoneham, *Theory of Defects in Solids: Electronic Structure of Defects in Insulators and Semiconductors* (Oxford University Press, 2001).

[2] M. W. Doherty, N. B. Manson, P. Delaney, F. Jelezko, J. Wrachtrup, and L. C. Hollenberg, The nitrogen-vacancy colour centre in diamond, Phys. Rep. **528**, 1 (2013).

[3] W. F. Koehl, B. B. Buckley, F. J. Heremans, G. Calusine, and D. D. Awschalom, Room temperature coherent control of defect spin qubits in silicon carbide, Nature (London) **479**, 84 (2011).

[4] M. Widmann, S.-Y. Lee, T. Rendler, N. T. Son, H. Fedder, S. Paik, L.-P. Yang, N. Zhao, S. Yang, I. Booker *et al.*, Coherent control of single spins in silicon carbide at room temperature, Nat. Mater. **14**, 164 (2015).

[5] F. Dolde, V. Bergholm, Y. Wang, I. Jakobi, B. Naydenov, S. Pezzagna, J. Meijer, F. Jelezko, P. Neumann, T. Schulte-Herbrüggen *et al.*, High-fidelity spin entanglement using optimal control, Nat. Commun. **5**, 3371 (2014).

[6] J. J. Pla, K. Y. Tan, J. P. Dehollain, W. H. Lim, J. J. Morton, F. A. Zwanenburg, D. N. Jamieson, A. S. Dzurak, and A. Morello, High-fidelity readout and control of a nuclear spin qubit in silicon, Nature (London) **496**, 334 (2013).

[7] F. Jelezko, T. Gaebel, I. Popa, M. Domhan, A. Gruber, and J. Wrachtrup, Observation of Coherent Oscillation of a Single Nuclear Spin and Realization of a Two-Qubit Conditional Quantum Gate, Phys. Rev. Lett. **93**, 130501 (2004).

[8] J. Cai, A. Retzker, F. Jelezko, and M. B. Plenio, A large-scale quantum simulator on a diamond surface at room temperature, Nat. Phys. **9**, 168 (2013).

[9] T. Unden, N. Tomek, T. Weggler, F. Frank, P. London, J. Zopes, C. Degen, N. Raatz, J. Meijer, H. Watanabe *et al.*, Coherent control of solid state nuclear spin nano-ensembles, npj Quantum Inf. **4**, 39 (2018).

[10] P. London, J. Scheuer, J.-M. Cai, I. Schwarz, A. Retzker, M. B. Plenio, M. Katagiri, T. Teraji, S. Koizumi, J. Isoya, R. Fischer, L. P. McGuinness, B. Naydenov, and F. Jelezko, Detecting and Polarizing Nuclear Spins with Double Resonance on a Single Electron Spin, Phys. Rev. Lett. **111**, 067601 (2013).

[11] E. Rej, T. Gaebel, T. Boele, D. E. Waddington, and D. J. Reilly, Hyperpolarized nanodiamond with long spin-relaxation times, Nat. Commun. **6**, 8459 (2015).

[12] A. J. Healey, L. T. Hall, G. A. L. White, T. Teraji, M.-A. Sani, F. Separovic, J.-P. Tetienne, and L. C. L. Hollenberg, Polarization Transfer to External Nuclear Spins Using Ensembles of Nitrogen-Vacancy Centers, Phys. Rev. Appl. **15**, 054052 (2021).

[13] P. Fernández-Acebal, O. Rosolio, J. Scheuer, C. Müller, S. Müller, S. Schmitt, L. McGuinness, I. Schwarz, Q. Chen, A. Retzker, B. Naydenov, F. Jelezko, and M. Plenio, Toward hyperpolarization of oil molecules via single nitrogen vacancy centers in diamond, Nano Lett. **18**, 1882 (2018).

[14] G. A. Álvarez, C. O. Bretschneider, R. Fischer, P. London, H. Kanda, S. Onoda, J. Isoya, D. Gershoni, and L. Frydman, Local and bulk ^{13}C hyperpolarization in nitrogen-vacancy-centred diamonds at variable fields and orientations, Nat. Commun. **6**, 8456 (2015).

[15] J. P. King, K. Jeong, C. C. Vassiliou, C. S. Shin, R. H. Page, C. E. Avalos, H.-J. Wang, and A. Pines, Room-temperature in situ nuclear spin hyperpolarization from optically pumped nitrogen vacancy centres in diamond, Nat. Commun. **6**, 8965 (2015).

[16] J. Scheuer, I. Schwartz, Q. Chen, D. Schulze-Sunninghausen, P. Carl, P. Hofer, A. Retzker, H. Sumiya, J. Isoya, B. Luy, M. B. Plenio, B. Naydenov, and F. Jelezko, Optically induced dynamic nuclear spin polarisation in diamond, New J. Phys. **18**, 013040 (2016).

[17] A. L. Falk, P. V. Klimov, V. Ivády, K. Szász, D. J. Christle, W. F. Koehl, A. Gali, and D. D. Awschalom, Optical Polarization of Nuclear Spins in Silicon Carbide, Phys. Rev. Lett. **114**, 247603 (2015).

[18] T. T. Tran, K. Bray, M. J. Ford, M. Toth, and I. Aharonovich, Quantum emission from hexagonal boron nitride monolayers, Nat. Nanotechnol. **11**, 37 (2016).

[19] H. L. Stern, Q. Gu, J. Jarman, S. Eizagirre Barker, N. Mendelson, D. Chugh, S. Schott, H. H. Tan, H. Sirringhaus, I. Aharonovich *et al.*, Room-temperature optically detected magnetic resonance of single defects in hexagonal boron nitride, Nat. Commun. **13**, 618 (2022).

[20] Z. Mu, H. Cai, D. Chen, J. Kenny, Z. Jiang, S. Ru, X. Lyu, T. S. Koh, X. Liu, I. Aharonovich, and W. Gao, Excited-State Optically Detected Magnetic Resonance of Spin Defects in Hexagonal Boron Nitride, Phys. Rev. Lett. **128**, 216402 (2022).

[21] A. Gottscholl, M. Diez, V. Soltamov, C. Kasper, A. Sperlich, M. Kianinia, C. Bradac, I. Aharonovich, and V. Dyakonov, Room temperature coherent control of spin defects in hexagonal boron nitride, Sci. Adv. **7**, eabf3630 (2021).

[22] A. Sajid, M. J. Ford, and J. R. Reimers, Single-photon emitters in hexagonal boron nitride: A review of progress, Rep. Prog. Phys. **83**, 044501 (2020).

[23] M. Abdi, J.-P. Chou, A. Gali, and M. B. Plenio, Color centers in hexagonal boron nitride monolayers: A group theory and ab initio analysis, ACS Photon. **5**, 1967 (2018).

[24] X. Gao, S. Vaidya, K. Li, P. Ju, B. Jiang, Z. Xu, A. E. L. Allcca, K. Shen, T. Taniguchi, K. Watanabe, S. A. Bhave, Y. P. Chen, Y. Ping, and T. Li, Nuclear spin polarization and control in a van der Waals material, Nat. Mater. **21**, 1024 (2022).

[25] F. T. Tabesh, Q. Hassanzada, M. Hadian, A. Hashemi, I. A. Sarsari, and M. Abdi, Strain induced coupling and quantum information processing with hexagonal boron nitride quantum emitters, Quantum Sci. Technol. **7**, 015002 (2022).

[26] T. Holstein and H. Primakoff, Field dependence of the intrinsic domain magnetization of a ferromagnet, Phys. Rev. **58**, 1098 (1940).

[27] P. Fernández-Acebal and M. B. Plenio, Sensing phases of water via nitrogen-vacancy centres in diamond, Sci. Rep. **8**, 13453 (2018).

[28] E. Lieb, T. Schultz, and D. Mattis, Two soluble models of an antiferromagnetic chain, Ann. Phys. (NY) **16**, 407 (1961).

[29] R. Baxter, *Exactly Solved Models in Statistical Mechanics* (Academic Press, London, 1982).

[30] W. Nolting and A. Ramakanth, *Quantum Theory of Magnetism* (Springer Science & Business Media, 2009).

[31] S. R. Hartmann and E. L. Hahn, Nuclear double resonance in the rotating frame, Phys. Rev. **128**, 2042 (1962).

[32] J. Johansson, P. Nation, and F. Nori, Qutip: An open-source python framework for the dynamics of open quantum systems, Comput. Phys. Commun. **183**, 1760 (2012).

[33] G. Cassabois, P. Valvin, and B. Gil, Hexagonal boron nitride is an indirect bandgap semiconductor, Nat. Photon. **10**, 262 (2016).

[34] A. Healey, S. Scholten, T. Yang, J. Scott, G. Abrahams, I. Robertson, X. Hou, Y. Guo, S. Rahman, Y. Lu *et al.*, Quantum microscopy with van der Waals heterostructures, Nat. Phys. **19**, 87 (2023).

[35] J.-P. Tetienne, Quantum sensors go flat, Nat. Phys. **17**, 1074 (2021).

[36] M. Abdi, M.-J. Hwang, M. Aghtar, and M. B. Plenio, Spin-Mechanical Scheme with Color Centers in Hexagonal Boron Nitride Membranes, Phys. Rev. Lett. **119**, 233602 (2017).

[37] M. Abdi and M. B. Plenio, Quantum Effects in a Mechanically Modulated Single-Photon Emitter, Phys. Rev. Lett. **122**, 023602 (2019).

[38] L. Song, L. Ci, H. Lu, P. B. Sorokin, C. Jin, J. Ni, A. G. Kvashnin, D. G. Kvashnin, J. Lou, B. I. Yakobson, and P. M. Ajayan, Large scale growth and characterization of atomic hexagonal boron nitride layers, Nano Lett. **10**, 3209 (2010).

[39] A. Gottscholl, M. Kianinia, V. Soltamov, S. Orlinskii, G. Mamin, C. Bradac, C. Kasper, K. Krambrock, A. Sperlich, M. Toth *et al.*, Initialization and read-out of intrinsic spin defects in a van der Waals crystal at room temperature, Nat. Mater. **19**, 540 (2020).

[40] *Quantum Mechanical Electronic Structure Calculations with Chemical Accuracy*, edited by S. Langhoff (Springer Netherlands, 2012).

[41] V. Ivády, G. Barcza, G. Thiering, S. Li, H. Hamdi, J.-P. Chou, Ö. Legeza, and A. Gali, Ab initio theory of the negatively charged boron vacancy qubit in hexagonal boron nitride, npj Comput. Mater. **6**, 41 (2020).

[42] A. Imamoğlu, E. Knill, L. Tian, and P. Zoller, Optical Pumping of Quantum-Dot Nuclear Spins, Phys. Rev. Lett. **91**, 017402 (2003).

[43] H. Christ, J. I. Cirac, and G. Giedke, Quantum description of nuclear spin cooling in a quantum dot, Phys. Rev. B **75**, 155324 (2007).

[44] Q. Chen, I. Schwarz, F. Jelezko, A. Retzker, and M. B. Plenio, Optical hyperpolarization of ^{13}C nuclear spins in nanodiamond ensembles, Phys. Rev. B **92**, 184420 (2015).